ROBUST CONTROL OF ENERGY MOMENTUM WHEELS SUPPORTED ON ACTIVE MAGNETIC BEARINGS USING $\mathscr{H}_\infty$ LOOP-SHAPING AND μ-SYNTHESIS

Alexander Lanzon [*] Panagiotis Tsiotras [*]

[*] *School of Aerospace Engineering, Georgia Institute of Technology, 270 Ferst Drive, Atlanta GA 30332-0150, USA.*

Abstract: The main objective of this research is to improve the feasibility of Energy Momentum Wheels for satellite systems through the development of robust LTI and gain-scheduled controllers for high-speed flywheel rotors supported on active magnetic bearings. A hybrid combination between $\mathscr{H}_\infty$ loop-shaping and μ-synthesis is used in this paper to design controllers. In order to reduce the computational complexity of the control designs and the order of the synthesized controllers, a method is devised in this paper to reduce the number of states that depend on the rotor speed. The rotor speed is treated as uncertainty in an LTI controller design and is used as a scheduling variable for a gain-scheduled framework. The success of the methodology used is demonstrated through numerical simulation and experimental results.

Keywords: Energy Momentum Wheels, Active Magnetic Bearings, Highly Flexible Systems, Robust Control, $\mathscr{H}_\infty$ Loop-Shaping, μ-Synthesis.

1. INTRODUCTION

An Energy Momentum Wheel (EMW) is a flywheel that combines the functions of energy storage and momentum management into a single component. The successful application of EMWs to satellite systems holds the promise of significantly reducing a satellite's mass and cost when contrasted with traditional satellite architecture that separates energy storage and momentum management functions (Proctor, 1999). Magnetic bearing technology is of crucial importance for efficient EMWs due to advantages that include very high operation speed, no lubrication requirement, no wear and low power loss. Spacecraft specifications often require very stringent pointing requirements as well as a vibration-free environment for onboard experiments. Imbalances and resonant modes in EMWs can create inertia forces which, when interacting with the stator, transmit unwanted vibration onto the spacecraft structure. This can be avoided with the use of active mag-

netic bearings (AMBs) coupled with an online controller that rejects undesirable vibrations (Knospe *et al.*, 1997). The successful development of an effective magnetic bearing controller is thus a critical technology for the use of EMWs in satellites.

Conventional control methodologies for flywheels supported on AMBs typically assume a Linear Time-Invariant (LTI) plant (Fujita *et al.*, 1993). This is a reasonable assumption if the speed of the rotor remains relatively constant. If, on the other hand, the speed of the rotor ranges over a wide spectrum of operating speeds, as is the case for EMWs, the LTI assumption is no longer valid. This is because the system matrix of these plants is a function of the rotor speed and the plant dynamics change considerably with rotor speed due to gyroscopic effects (Tsiotras and Mason, 1996). Consequently, conventional control algorithms which do not give due consideration to the parameter varying nature of the plant often do not have the desired performance when operated on a wide range of rotor speeds.

The greatest difficulty in designing controllers with good robust performance margins for EMWs operating at high rotor speeds is the highly flexible nature of the vibrational modes. The proximity of the poles and zeros of such plants to the imaginary axis imposes fundamental limitations on the achievable performance (Francis, 1987). This, together with the parameter-varying nature of the plant and the very strict disturbance rejection specifications, makes ad-hoc or trial-and-error designs inadequate.

In this paper, a hybrid scheme between $\mathscr{H}_\infty$ loop-shaping and μ-synthesis is used to design robust controllers. Performance requirements are specified through loop-shaping weights whereas robustness to parametric uncertainty is incorporated through a μ-synthesis design.

2. SYSTEM DESCRIPTION

An experimental test rig was designed and constructed at the University of Virginia that possesses all important features of EMWs that will be used onboard satellites (Schönhoff *et al.*, 2000). A schematic diagram of this test rig is shown in Figure 1. This test rig is used to study/validate de-
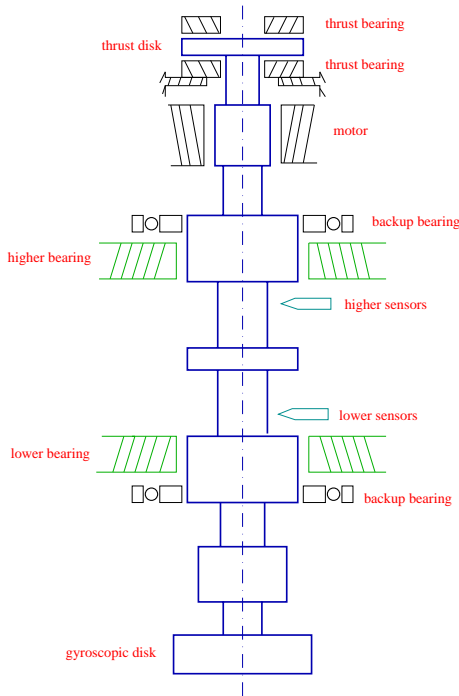

Fig. 1. Schematic diagram for an EMW test rig

signed controllers. The test rig was designed in an overhanging configuration, as shown in Figure 1. The thrust magnetic bearing, which supports the rotor vertically, is located at the top. Two sets of radial magnetic bearings are located in the middle of the rotor shaft, with one set labeled as higher bearing and the other set labeled as lower bearing. An additional set of mechanical bearings, located

next to the radial magnetic bearings, are used as backup bearings. Eddy-current displacement probes are used to pick up the displacement signals of the rotor. The design also completely integrates the motor with the rotor shaft. A gyroscopic disk, simulating the gyroscopic effects of a flywheel, is located at the bottom.

Besides all the mechanical parts just described, the system also consists of amplifiers for the actuators, sensors and anti-alias filters for digital control. Furthermore, interaction of this system with the surrounding structure is modeled by a substructure transfer function. The block diagram for the closed-loop system is shown in Figure 2. In order to
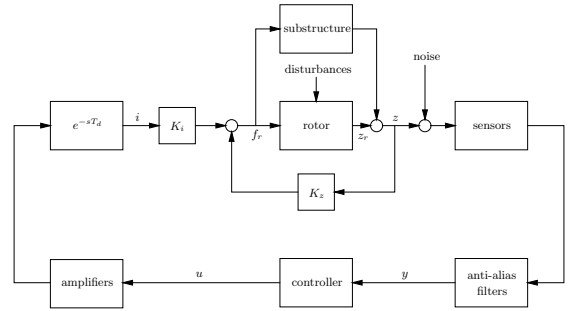

Fig. 2. Block diagram for the closed-loop system

have effective model-based control designs, accurate mathematical models were developed for each component in the physical system and validated through extensive experimental testing.

2.1 *Nominal Plant Model*

The final reduced order model that includes all the plant components in Figure 2 has 44 states and can be described by:

$$\dot{x} = (A_o + \rho A_g)x + Bu,$$
$$y = Cx,$$

where ρ is the rotor spin speed, u is control input and y is the vector of measured outputs. The plant dynamics posses several features which make the control problem challenging from both a theoretical and an experimental stand-point. This is because the plant:

(i) is unstable and non-minimum phase,
(ii) has non-negligible time-delay,
(iii) is highly flexible with several flexible modes inside the desired closed-loop bandwidth,
(iv) is an LPV system with the rotor spin speed ρ as parameter,
(v) has significant uncertainty on the natural frequencies of the flexible modes.
(vi) has significant unmodeled substructure dynamics.

These features, together with the required stringent performance specifications, demand for advanced control algorithms which are capable of

handling these difficulties in a non-conservative and systematic way.

The gyroscopic variations which depend on ρ arise only in the modeling of the rotor dynamics and thus the matrix A_g is rank deficient. In fact, for the test rig of Figure 1, the rank of A_g is 10 whereas its dimension is 44×44. Due to this property, it is possible to decompose A_g into $A_g = B_g C_g$ where the number of columns of B_g and the number of rows of C_g are equal to the rank of A_g (Horn and Johnson, 1996). Using this decomposition, the parameter ρ may be pulled-up in an LFT setup as shown in Figure 3, where r denotes the rank of A_g.
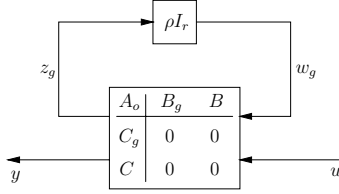

Fig. 3. Nominal plant with ρ pulled-up in LFT setup

The singular values of the nominal plant plotted against frequency at four different values of the parameter ρ are depicted in Figure 4. These singular
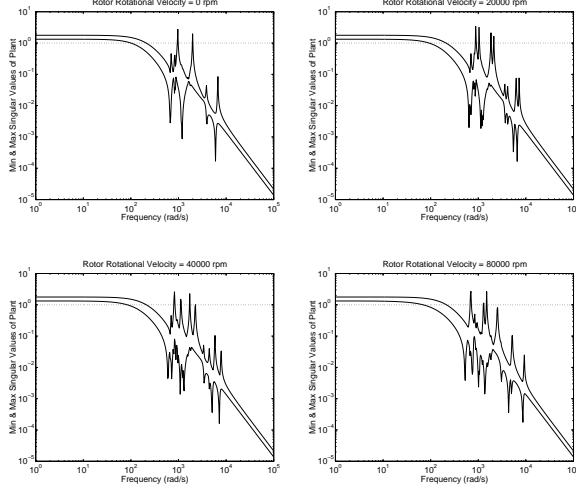

Fig. 4. Singular values of plant dynamics

value plots clearly illustrate the level of flexibility and the non-trivial variation of the plant with the parameter ρ.

2.2 Perturbed Plant Model

In order for a controller to perform well on a physical plant, the uncertainty characterization around the nominal plant model must be such that it captures the dynamics of the true plant. The predominant source of uncertainty in EMW systems occurs in the knowledge of the natural frequencies of the vibrational modes. Since even small mismatches in the natural frequencies of

vibrational modes can induce very large additive, multiplicative or coprime factor errors, it is of crucial importance to capture this type of uncertainty directly as parametric uncertainty (Balas and Young, 1995).

Towards this end, let A be the system matrix in the nominal plant model. Then, A can be transformed to a real modal representation $\tilde{A} = TAT^{-1}$ through a similarity transformation matrix T. Then the 2×2 block corresponding to the i-th vibrational mode on the main diagonal of $\tilde{A}$ is of the form

$$\tilde{A}_i = \begin{bmatrix} 0 & 1 \\ -[\omega_i(1+\delta_i)]^2 & -2\xi_i[\omega_i(1+\delta_i)] \end{bmatrix},$$

where ξ_i is the modal damping of the i-th mode, which is assumed to be well-known, and ω_i is the natural frequency of the i-th mode with relative multiplicative uncertainty δ_i. Linearizing the term $[\omega_i(1+\delta_i)]^2$ for small uncertainties δ_i gives $\omega_i^2 + 2\omega_i^2\delta_i$ and hence $\tilde{A}_i$ can be rewritten as

$$\tilde{A}_i = \begin{bmatrix} 0 & 1 \\ -\omega_i^2 & -2\xi_i\omega_i \end{bmatrix} + \begin{bmatrix} 0 \\ 1 \end{bmatrix} \delta_i \begin{bmatrix} -2\omega_i^2 & -2\xi_i\omega_i \end{bmatrix}.$$

Thus, $\tilde{A}_i$ can be represented in an LFT setup with the input and output vectors

$$\tilde{B}_i = \begin{bmatrix} 0 \\ 1 \end{bmatrix} \quad \text{and} \quad \tilde{C}_i = \begin{bmatrix} -2\omega_i^2 & -2\xi_i\omega_i \end{bmatrix}$$

and a single real uncertainty δ_i. In order to keep the numerical condition of the original plant model, the plant model is not transformed to the modal coordinates. Instead, the input and output uncertainty matrices $\tilde{B}$ and $\tilde{C}$, assembled from the vectors $\tilde{B}_i$ and $\tilde{C}_i$, are transformed back to the original coordinates: $C_d = \tilde{C}T$ and $B_d = T^{-1}\tilde{B}$. The numeric conditioning of the input and output uncertainty matrices is further improved by scaling the rows and columns of C_d and B_d respectively, to have equal 2-norms. The perturbed plant model so achieved is depicted in Figure 5. For the test rig a $\pm 6\%$ uncertainty on the nat-
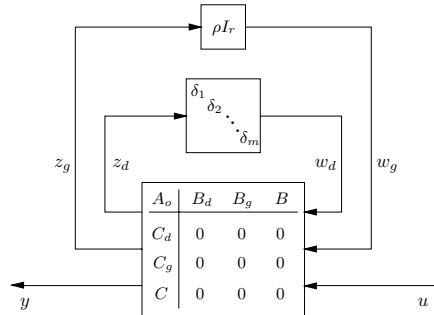

Fig. 5. Perturbed plant with parametric uncertainty

ural frequencies of the 20 vibrational modes was considered adequate.

3. CONTROL PROBLEM FORMULATION

Given a nominal plant model for an EMW system and an uncertainty characterization as illustrated in Figure 5, the control problem is cast into an $\mathscr{H}_\infty$ loop-shaping design problem as depicted in Figure 6. This is not a standard $\mathscr{H}_\infty$ loop-shaping
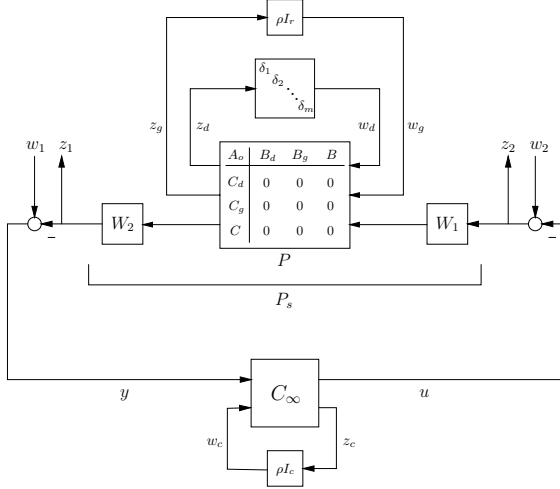

Fig. 6. Block diagram for $\mathscr{H}_\infty$ loop-shaping framework

problem because of the parametric uncertainty on the nominal plant P. It should be clear from Figure 6 that setting $c = 0$ gives an LTI controller (independent of the parameter ρ), whereas setting $c > 0$ gives a Gain-Scheduled controller that is a function of ρ.

Loop-shaping weights W_1 and W_2 are usually designed in two stages. In the first stage, the desired loop-shape is determined. This usually involves translating time-response requirements and closed-loop performance specifications into the frequency domain. To do this, engineers largely rely on their intuition and their past experience with loop-shaping concepts. In the second stage, the designer selects loop-shaping weights W_1 and W_2 so that P_s has the desired loop-shape.

Since P_s is a function of ρ in the block diagram of Figure 6, selecting loop-shaping weights that are independent of ρ means that a ρ-independent performance/stability level is demanded from the closed-loop system. The loop-shaping weights selected for the test rig are shown in Figure 7. For
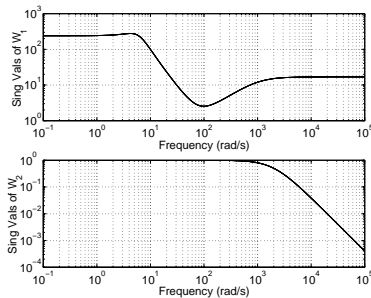

Fig. 7. Loop-shaping weights W_1 and W_2

this problem, diagonal weights were found to be sufficient. These loop-shaping weights satisfy the desired specifications (e.g. sensitivity and compliance reduction of the order of 100 at low frequency, closed-loop bandwidth around 1000 `rad/s` and reduction of spill-over dynamical uncertainty beyond 3000 `rad/s`).

In order to synthesize C_∞, the block diagram of Figure 6 is redrawn into an LFT configuration as shown in Figure 8. Here, G is the general-
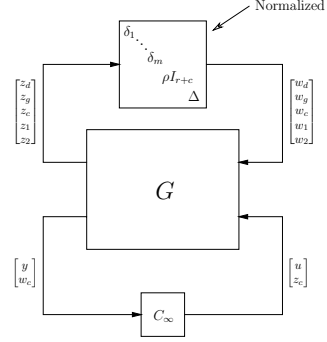

Fig. 8. LFT interconnection for C_∞ synthesis

ized plant and consists of all known or specified transfer functions in the feedback interconnection, C_∞ is the controller map to be synthesized, and diag $[\delta_1, \ldots, \delta_m, \rho I_{r+c}, \Delta]$ is the normalized structured uncertainty block in the system. It should be clear that if $c = 0$, the signals w_c, z_c and the corresponding sub-blocks in C_∞, G and the uncertainty block disappear from the formulation.

Since the structured uncertainty block in Figure 8 is normalized to have size less than or equal to unity, a necessary and sufficient condition for robust performance of this interconnection is that

$$\sup_{\omega \in \mathbb{R}} \mu_{\mathbf{\Delta}_{TOT}} \big[\mathcal{F}_l \left(G(j\omega), C_\infty(j\omega) \right) \big] < 1,$$

where $\mathbf{\Delta}_{TOT}$ determines the structure of the uncertainty block. The problem of synthesizing C_∞ thus reduces to a standard μ-synthesis problem which can be solved through D-K iterations.

4. REDUCTION OF NUMBER OF PLANT STATES DEPENDING ON ρ

Consider the problem of synthesizing C_∞ using the D-K iterative procedure for the problem depicted in Figure 8. Note that one of the uncertainty blocks is ρI_{r+c}. Corresponding to this uncertainty block, there will be a full-block D-scale which has dimension $(r+c) \times (r+c)$. In a typical D-K iterative procedure, the D-scales are first computed pointwise in frequency and then the resulting frequency data for each element is fitted by a transfer function in order to construct a rational D-scale that can be used for controller synthesis. If $(r + c)$ is not a small number, this procedure may easily result in a rational D-scale that has very high

order. Such a high order D-scale will then, in turn, result in a high order synthesized C_∞. Thus, it is evident that the design procedure will greatly benefit if $(r + c)$ can be reduced in any way with minor compromise in the modeling accuracy and achieved performance.

Since from an engineering point-of-view c will always be chosen to be less than or equal to r, the problem reduces to finding the smallest value of r for which there is only minor compromise in the modeling accuracy of the plant. The basis of such a reduction will rely on the ν-gap metric.

Towards this end, consider again the nominal plant model depicted in Figure 3 and let the choices of B_g and C_g in the decomposition of $A_g = B_g C_g$ be as follows:

$$B_g := U \begin{bmatrix} \Theta \\ 0 \end{bmatrix} \quad \text{and} \quad C_g := \begin{bmatrix} I_r & 0 \end{bmatrix} U^T,$$

where $A_g = U \begin{bmatrix} \Theta & 0 \\ 0 & 0 \end{bmatrix} U^T$ is a Real Schur Decomposition with U satisfying $UU^T = U^T U = I$ and

$$\Theta = \operatorname*{diag}_{i=1}^{r/2} \left(\begin{bmatrix} 0 & \sigma_i \\ -\sigma_i & 0 \end{bmatrix} \right)$$

with $\sigma_1 \geq \sigma_2 \geq \cdots \geq \sigma_{r/2} > 0$. Note that Θ takes this special form because A_g is skew-symmetric (i.e. $A_g = -A_g^T$) for EMW systems (Merkin, 1956). Then, define a new plant model $\hat{P}_q$ as depicted in Figure 9. The only difference between
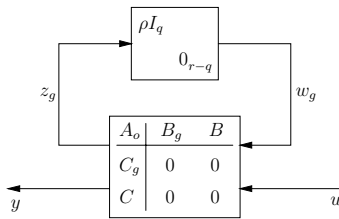
Fig. 9. Reduction in number of states that depend on ρ

$\hat{P}_q$ and the nominal plant model P depicted in Figure 3 is the number of states that depend on the parameter ρ. The following procedure was used to determine the smallest value of q such that the systems $\hat{P}_q$ and P are close in a feedback sense:

1. Let $q = r - 1$.
2. Evaluate $\delta_\nu(W_2 P W_1, W_2 \hat{P}_q W_1)$ at every ρ in the operating envelope.
3. If $\delta_\nu(W_2 P W_1, W_2 \hat{P}_q W_1) \ll b_{opt}(W_2 P W_1)$ at each ρ, then let $q = q - 1$ and go back to Step 2. Otherwise EXIT.

The plots in Figure 10 are the results of this procedure when applied to the test rig nominal plant. Since experience suggests (McFarlane and Glover, 1992) that 0.3 is a good value for $b_{opt}(W_2 P W_1)$, it follows from Figure 10 that $q = 8$ is the smallest value of q such that $\hat{P}$ and P are close in a feedback sense. This implies a reduction of 2 states (since $r = 10$) from the dependence on ρ
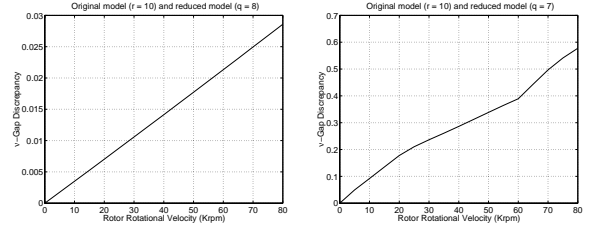
Fig. 10. ν-gap discrepancy evaluated at every ρ

which yields considerable computational improvement as there are 64 elements for the D-scale associated with ρI_q when compared to 100 elements for the D-scale associated with ρI_r. Consequently, Figures 6 and 8 are redrawn with $\operatorname{diag}\begin{bmatrix} \rho I_q, 0_{r-q} \end{bmatrix}$ replacing ρI_r in the uncertainty blocks.

5. LTI CONTROLLER SYNTHESIS AND RESULTS

An LTI controller was synthesized for the test rig by setting $c = 0$ in Figures 6 and 8 using the approach of the previous sections. This controller has 56 states and achieves robust performance in the face of the following specified uncertainties:

- 6% parametric uncertainty on the natural frequency of the vibrational modes,
- 0 to $25,000$ `rpm` as allowed parameter variations in ρ,
- 20% unstructured uncertainty on the normalized coprime factors of the shaped plant.

Figure 11 shows the singular value plots for C_∞ and the controller C. It can be seen that the con-
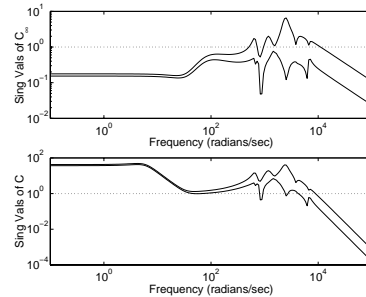
Fig. 11. Controller singular value plots

troller C has high gain at low frequency to achieve the desired sensitivity and compliance reduction, introduces some phase lead around cross-over to improve the robust stability margins and rolls-off rapidly after 5000 `rad/s` to reduce the effects of spill-over dynamics. The complex dynamical changes in the controller around cross-over are due to the vibrational modes in the plant, since lightly damped poles and zeros around cross-over can be detrimental to stability if the controller does not adequately compensate for them. This controller worked well in simulation on the high-fidelity plant model, and the experimental results were also very comparable.

The compliance magnitude responses obtained during experiment are given in Figure 12 and the
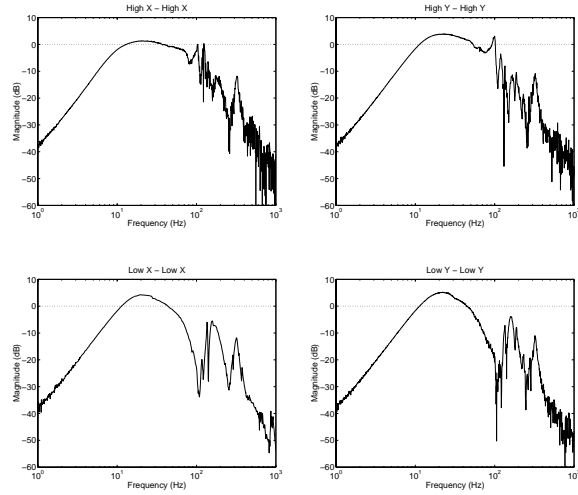

Fig. 12. Magnitude plots of $(I - PC)^{-1}P$

plant input disturbance rejection time responses for a step disturbance of unit magnitude are shown in Figure 13. The only shortcoming of this LTI ro-
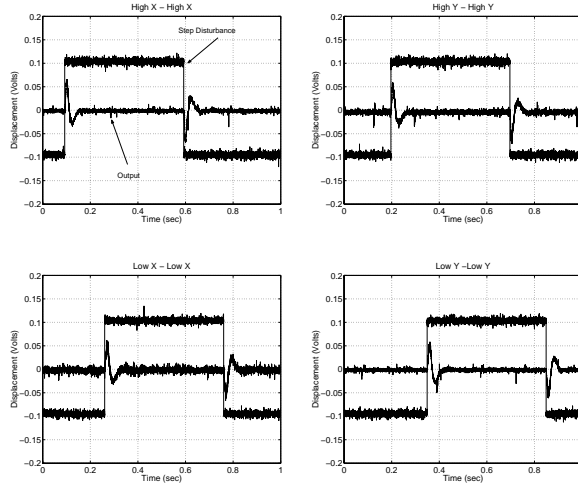

Fig. 13. Disturbance rejection time response

bust controller design is that the parameter range of ρ stabilized by this one LTI controller is not as wide as required for a typical EMW system.

Consequently, a gain-scheduled robust controller may be designed by setting $c > 0$ in Figures 6 and 8. The structure of this controller:

$$\dot{x}_k = (A_{k_o} + \rho A_{k_g})x_k + B_k y$$
$$u = C_k x_k$$

with $\mathrm{rank}(A_{k_g}) = c$ would be very similar to that of the plant. The synthesis of this gain-scheduled controller would be based on the assumption that the parameter ρ varies very slowly, although it spans a wide range of rotor spin speeds. This assumption is true for most EMW applications and hence justifies the approach. Furthermore, since ρ varies so slowly and $\dot{\rho}$ is not available for measurement, existing LPV designs would give quite conservative results.

6. CONCLUSIONS

Experience with highly flexible systems shows that unstructured uncertainty does not capture well perturbations on the natural frequencies of the vibrational modes around cross-over. This is because the proximity of these lightly damped poles and zeros to the imaginary axis induces very large unstructured uncertainties in a gap sense. Consequently, a combination of parametric (structured) and unstructured uncertainty was used in this paper to correctly model the dynamics of a highly flexible rotating structure supported on magnetic bearings. The rotor speed was treated as uncertainty so as to increase the robustness of the synthesized controller against such variations. Experiments confirmed the good stability and performance characteristics of the proposed control design.

7. REFERENCES

Balas, G. J. and P. M. Young (1995). Control design for variations in structural natural frequencies. *Journal of Guidance, Control and Dynamics* **18**(2), 325–332.

Francis, B. A. (1987). *A course in $\mathscr{H}_\infty$ control theory*. Vol. 88 of *Lecture notes in Control and Information Sciences*. first ed.. Springer-Verlag.

Fujita, M., K. Hatake and F. Matsumura (1993). Loop shaping based robust control of a magnetic bearing. *IEEE Control Systems Magazine* **13**(4), 57–65.

Horn, R. A. and C. R. Johnson (1996). *Matrix Analysis*. Cambridge University Press.

Knospe, C. R., S. M. Tamer and J. Lindlau (1997). New results in adaptive vibration control. In: *Proceedings of MAG '97 Industrial COnference and Exhibition on Magnetic Bearings*. Alexandria, VA. pp. 209–219.

McFarlane, D. and K. Glover (1992). A loop shaping design procedure using $\mathscr{H}_\infty$ synthesis. *IEEE Transactions on Automatic Control* **37**(6), 759–769.

Merkin, D. R. (1956). *Gyroscopic Systems*. Gostekhizdat. Moscow.

Proctor, P. (1999). Flywheels show promise for 'high-pulse' satellites. *Aviation Week and Space Technology* p. 67.

Schönhoff, U., J. Luo, G. Li, E. Hilton, R. Nordmann and P. Allaire (2000). Implementation results of μ-synthesis control for an energy storage flywheel test rig. In: *Proceedings of the 7th International Symposium on Magnetic Bearings*. Zurich, Switzerland.

Tsiotras, P. and S. Mason (1996). Self-scheduled $\mathscr{H}_\infty$ controllers for magnetic bearings. In: *International Mechanical Engineering Congress and Exposition*. Atlanta, GA. pp. 151–158.